Original Research Article

Insertion of the $MnSnI_3$ and $CsGeI_3$ Two Absorber Layers in Order to Perform the Photovoltaic Behavior of the Perovskite Solar Cell

Abdullah Belbia[1], Keltoum Dris[1], Mostefa Benhaliliba*[,1], Abbas Ayeshamariam[2]

[1]*Film Device Fabrication-Characterization and Application FDFCA Research Group USTOMB, 31130 Oran, Algeria*

[2]*Department of Physics, Khadir Mohideen College, Adirampattinam, Thanjavur District, Tamil Nadu 614701, India*

Citation M. Benhaliliba. Insertion of the $MnSnI_3$ and $CsGeI_3$ Two Absorber Layers in Order to Perform the Photovoltaic Behavior of the Perovskite Solar Cell. *J. Eng. Ind. Res.* **2025**, 6 (3):195-210.

https://doi.org/10.48309/jeires.2025.512985.1181

Article info:
Submitted: 2025-03-17
Revised: 2025-04-19
Accepted: 2024-05-01
ID: JEIRES-2503-1181

Keywords:
Lead-free perovskite solar cells; $MnSnI_3/CsGeI_3$; SCAPS-1D; Photovoltaic parameters; Defect density optimization; High efficiency photovoltaic.

ABSTRACT

This study suggests novel lead-free perovskite solar cell architecture with double absorber layers of $CsGeI_3$ and $MASnI_3$ to eliminate lead toxicity while maintaining high efficiency. Using SCAPS-1D simulations, critical parameters- absorber layer thickness, doping density, and defect density- were systematically optimized to enhance photovoltaic performance. The optimized structure (FTO/ZnO/$MASnI_3$/$CsGeI_3$/NiO) achieved a power conversion efficiency (PCE) of 32.07%, with an open-circuit voltage (Voc) of 1.166 V, Short-circuit current density (Jsc) of 30.72 mA/cm^2, and fill factor (FF) of 89.52%. Key findings reveal that a 1200 nm thickness for both $CsGeI_3$ and $MASnI_3$ layers maximizes light absorption and carrier generation, while a doping density of 10^{20} cm^{-3} strengthens the built- in electric field, improving charge separation. Defect density optimization highlights the critical role of the $MASnI_3$layer, where reducing defects to 10^{12} cm^{-3} minimizes the recombination losses. Interface defect densities at NiO/$CsGeI_3$, $CsGeI_3$/$MASnI_3$, and $MASnI_3$/ZnO were optimized to 10^{10} cm^{-3}, with $MASnI_3$/ZnO exhibiting the highest sensitivity to defects. This work demonstrates the viability of lead-free perovskites for high-efficiency solar cells. The results pave the way for experimental validation and scalable production, aligning with safe renewable energy purposes.

Introduction

Despite the remarkable development that we have recently seen in perovskite solar cells technology, since it may offer a good alternative to traditional silicon-based cells due to their cost-effectiveness, and easiness of fabrication process, while maintaining high performance [1-2], several challenges still face its commercial reliability, the major challenges are the stability and the toxicity [3]. This stability is affected by different issues, including the impact of moisture, ultraviolet radiation, ion migration, and thermal stress, which can lead to performance degradation over time,

*Corresponding Author: Mostefa Benhaliliba (mbenhaliliba@gmail.com)

making them less reliable compared to traditional solar cell technologies. Furthermore, Perovskite materials often contain lead, which has environmental and health impacts during production or application [4]. Therefore, ongoing research has led to innovative methods to control this instability. Studies have shown that the charges transport layers have a prominent effect on stability and efficiency, Ain *et al.* [5] suggested that using Hexakis triphenylene discotic liquid crystal as a HTL offers enhanced ambient and thermal stability. Di Girolamo *et al.* [6] demonstrated that the introduction of a hybrid Mg-organic layer between NiO_X and Perovskite layers removes dark hysteresis, improving stability and even yield. The fabrication techniques of perovskite materials also take a step forward, Bai *et al.*[7] increased the stability by integrating ionic liquids in the film of perovskite. Similarly, Shangshang *et al.* [8] incorporated benzyl hydrazine hydrochloride, mitigating ion migration, protecting the sensitive perovskite layer is a key strategy for enhancing stability, polymers, metal oxides (e.g., TiO, SnO, and ZnO), and organic/inorganic hybrids (such as SiO-TiO), these protective barriers are crucial for preventing degradation, as well as encapsulation exhibits essential role in improving PSCs stability [4].

Notably, innovative encapsulation techniques have enabled the majority of PSCs to meet the IEC standards in whole or in part [9]. Recent advancements in corrosion resistant coatings, such as Zn-TiO_2 nanocomposition, further highlight the potential of material engineering for long-term device durability [10]. Moreover, the tolerance factor Goldschmidt is a valuable tool for assessing the structural stability of perovskite materials, by targeting specific values, the Goldschmidt factor aids in selecting appropriate cations for perovskite structures, ensuring that the chosen materials will maintain stability under operational conditions [11]. To solve the toxicity issue of Lead-based perovskites, recent research replaced lead ions in perovskite compounds with nontoxic materials such as germanium or tin. Unfortunately, these lead-free perovskite materials have not yet reached the yields of lead-based perovskite [4,12].

However, this study presents a novel perovskite solar cell structure, developed and optimized to address this issue, combining different perovskite materials bilayer solar cells can absorb a wide range of sunlight spectrum, and hence high-power conversion efficiencies would be achieved. This cell had the configuration (FTO/ZnO/$MASnI_3$/$CsGeI_3$/NiO). Methylammonium tin tri-iodide ($MASnI_3$) with its non-toxic nature and optoelectronic properties, such as the direct bandgap (1.2 eV), and the high carriers mobility, among the best lead-free perovskites currently considered [13-14].Cesium germanium tri-iodide ($CsGeI_3$) is being explored for use due to its favorable electronic properties and stability [15]. NiO is a key HTL in PSCs, known for its stability, photostability, and excellent optical properties [6,16]. ZnO remains a promising ETL in perovskite solar cells, for its large band-gap and low-temperature deposition, FTO is used as front contact [11].

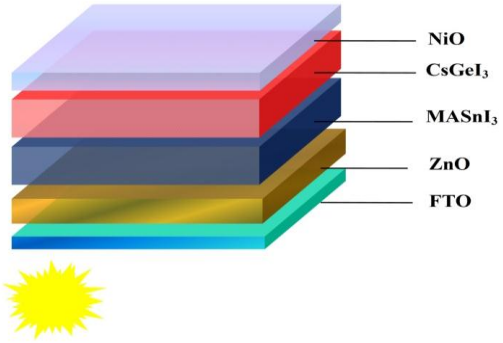

Figure 1: Structure of (NiO/$CsGeI_3$/$MASnI_3$/ZnO/FTO).

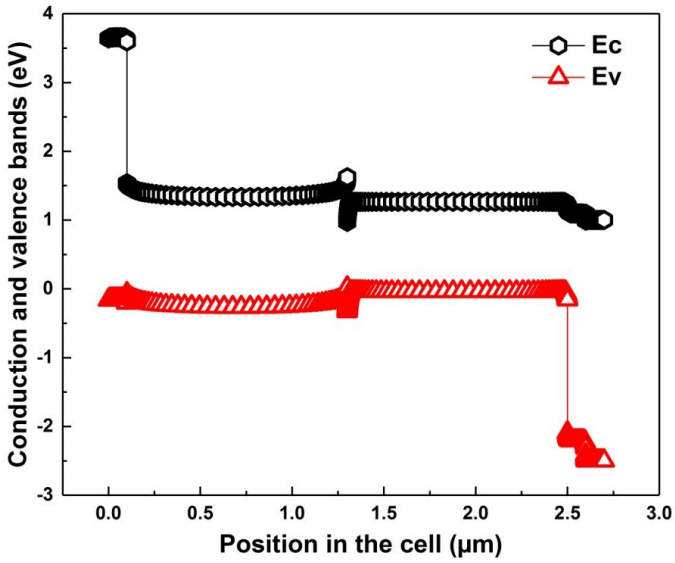

Figure 2: Diagram of energy band.

Methods of Computation

Computational tool (SCAPS-1D)

Fabrication of different layers in a multilayer PSC can be both costly and time-consuming, presenting significant challenges in the development of efficient solar cell technologies. As a result, simulation has emerged as an effective research method that aids in understanding the complexities of experimental systems like PSCs. Several photovoltaic technology simulation programs have been developed, including GGPVDM, AMPS, SILVACO, SCAPS, and TCAD. SCAPS-1D is recognized for its reliability in modeling solar cell devices. Developed at the Electronics and Information Systems (ELIS) department in Ghent University. SCAPS-1D developed initially for CdTe and $CuInSe_2$ solar cells, but it is also used for PSCs because of modifications that were added later. This software is capable of simulating up to7 layers and various parameters: thickness, light absorption, distribution of energy, doping profile, and concentration of charge carriers, which is crucial for optimizing the PSCs performance. By finding numerical solutions of three differential equations constituting the basic semiconductor equations [11,17-19].

The Poisson equation [11,18]:

$$-\frac{\partial}{\partial x}\left[-\varepsilon(x)\frac{\partial V}{\partial x}\right] = q[p(x) - n(x) + N_D^+(x) - N_A^-(x) + p_t(x) + n_t(x)] \quad (1)$$

The hole continuity equation [11,18]:

$$\frac{\partial p}{\partial t} = \frac{1}{q}\frac{dJ_p}{dx} + G_p - R_p \quad (2)$$

The electron continuity equation [11,18]:

$$\frac{\partial n}{\partial t} = \frac{1}{q}\frac{dJ_n}{dx} + G_n - R_n \quad (3)$$

Where,

⍰: dielectric permeability

q: the charge

V: the potential

p(x): concentration of free holes

n(x): concentration of free electrons

$N_A^-(x)$: ionized acceptor concentration

$N_D^+(x)$: ionized donor concentration

G_p: holes generation rate

G_n: electrons generation rate

$n_t(x)$: electron trap density

$p_t(x)$: hole trap density

R_p: holes recombinant rate

R_n: electrons recombination rate

J_p: holes current density

J_n: electrons current density

Optimization strategy

The main objective of this simulation is to perform the photovoltaic behavior of this new suggested cell, studying the efficiency of the device in various thicknesses, doping densities,

Table 1: Initial input of ($MASnI_3$, $CsGeI_3$, ZnO, NiO, and FTO) materials in cell simulation

Parameters	NiO	$CsGeI_3$	$MASnI_3$	ZnO	FTO
Thickness (nm)	*100*	500	500	100	100
Band gap (eV)	3.8	1.6	1.3	3.3	3.5
Electron affinity (eV)	1.46	3.52	4.17	4.1	4
Dielectric permittivity (relative)	11.7	18	8.2	9	9
CB effective density of states (cm^{-3})	2.5×10^{20}	1×10^{18}	2.8×10^{18}	4×10^{18}	2.2×10^{18}
VB effective density of states (cm^{-3})	2.5×10^{20}	1×10^{18}	3.9×10^{18}	1×10^{19}	1.8×10^{19}
Electron thermal velocity (10^7cm s^{-1})	1	1	1	1	1
Hole thermal velocity (10^7cm s^{-1})	1	1	1	1	1
Electron mobility (cm^2 V^{-1} s^{-1})	2.8	20	1.6	100	20
Hole mobility (cm^2 V^{-1} s^{-1})	12	20	1.6	25	10
Shallow uniform donor density N_D ($10^{18}cm^{-3}$)	0	0	0	1	20
Shallow uniform acceptor density N_A(10^{18} cm^{-3})	1	1	1	0	0
N_t (10^{14} cm^{-3}) total	1	1	1	10	100
Ref.	[20]	[15]	[13]	[21]	[22]

Table 2: Initial input for NiO/$CsGeI_3$, $CsGeI_3$/$MASnI_3$, and $MASnI_3$/ZnO interfaces

Interface layer	NiO/$CsGeI_3$	CsGeI3/$MASnI_3$	$MASnI_3$/ZnO
Type of defect	neutral	neutral	neutral
Electrons capture cross-section (cm^2)	1×10^{-19}	1×10^{-19}	1×10^{-19}
Hole capture cross-section (cm^2)	1×10^{-19}	1×10^{-19}	1×10^{-19}
Energy distribution	single	single	single
Defect energy level reference (E_t)	Above highest EV	Above highest EV	Above highest EV
Energy level related to reference (eV)	0.6	0.6	0.6
Total density integrated over all energies (cm^{-3})	**1×10^{10}**	**1×10^{10}**	**1×10^{10}**

and defect densities of $MASnI_3$ and $CsGeI_3$ layers, and interfaces defect densities.

Initial parameters

The two following tables present the initial input of our structure in AM1.5G solar spectrum, T=300 K, and power density of 1000 $W.m^{-2}$ [11,18].

Results and Discussion

Optimization of $CsGeI_3$ and $MASnI_3$ thickness

The thickness of layers in solar cells is crucial as it influences photon absorption, charge carriers generation and stability [23].

Optimizing layer thickness can enhance power conversion efficiency while minimizing recombination losses, leading to improved overall cell performance [24]. In this part of our study, we investigated how varying the thickness of the two active layers affect our cell performance, by testing it in a range of 100 nm to 1200 nm (while keeping other initial inputs the same) the results demonstrated significant improvement in all the four main characteristics of the cell:

Power conversion efficiency (PCE), Fill factor (FF), Short circuit current density (Jsc), and Open circuit voltage (Voc). The increase of $CsGeI_3$ layer thickness from 100 nm to 1200 nm improved photovoltaic parameters: Voc rose from 1.050142 V to 1.05065 V, Jsc from 27.92034661 $mA.cm^{-2}$ to 28.14728004 mA cm^{-2}, FF from 85.8138% to 85.3875%, and PCE25.1609% to 25.3875% (Figure 3). At this optimal thickness ($CsGeI_3$:1200 nm) the optimization of $MASnI_3$ thickness lead to a significant improvement reaches: Voc=1.052831 V, Jsc=31.05579789 mA cm^{-2}, FF=86.8970%, and PCE=28.4123% for a thickness of 1200 nm (Figure 4).

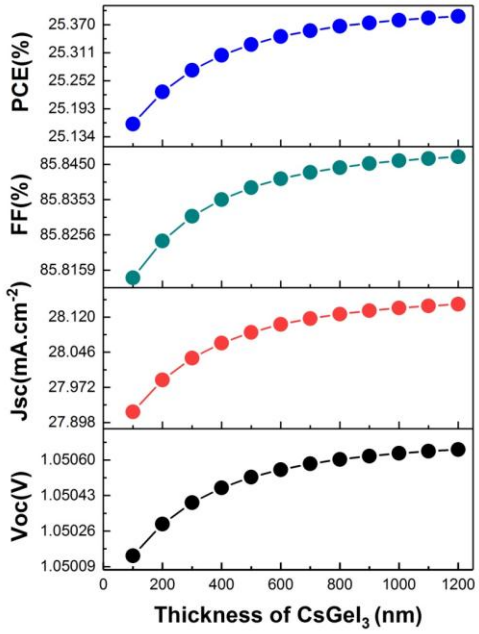

Figure 3: The photovoltaic characteristics as a function of $CsGeI_3$ layer thickness.

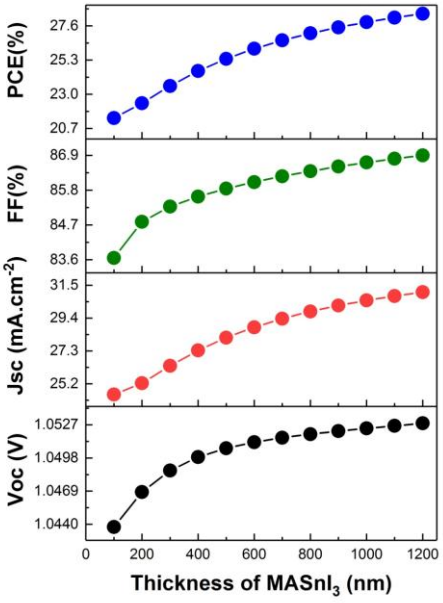

Figure 4: The photovoltaic characteristics as a function of $MASnI_3$ layer thickness.

When we increase the thickness of the active layer, the amount of light absorbed increases, resulting in better generation of electron-hole pairs, this means that more excitons can contribute to the current, leading to improved solar cell performance.

Optimization of $MASnI_3$ and $CsGeI_3$ doping density

Doping is essential to optimize the PSCs performance by enhancing charge transport, improving the voltage at open circuit (Voc) and increasing conversion rate [25], it modifies the electronic properties of perovskite materials, leading to better performance and stability in solar cell applications [26-28]. To know the Impact of doping density in $CsGeI_3$ and $MASnI_3$absorber layer on the cell proposed, we varied the doping densities of each layer from 10^{10} to 10^{20} cm^{-3}.

For $CsGeI_3$ layer

From 10^{10} to 10^{18} cm^{-3}, there is almost no change in the photovoltaic parameters, for values greater than $10^{18}cm^{-3}$they rise to an optimal value: Voc=1.061825 V, Jsc=32.90052382 mA cm^{-2}, FF=87.8326%, and PCE=30.6840% for a doping density of 10^{20} cm^{-3} (Figure 5).

To figure out the reason for this result we analyzed the electric field distribution in the cell for doping density of 10^{12} cm^{-3} and 10^{20} cm^{-3} in the $CsGeI_3$ layer, the resulting graphs are illustrated in Figure 6.

The results obtained from the graph reveal that at a doping density of 10^{20} cm^{-3} the electric field at the NiO/$CsGeI_3$ interface is stronger compared to lower doping levels, this high electric field enhances the separation and collection of generated carriers, leading to improved cell performance. We adopted this density for the remaining measures.

For the MASnI3 layer

According to the graphs (Figure 7), the PV parameters remain constant less than 10^{14} cm^{-3}. beyond 10^{14} cm^{-3} Voc, PCE, and FF increase steadily up to 10^{20} cm^{-3}, while the Jsc decrease up to Jsc=30 mA cm^{-2} for 10^{20} cm^{-3}. As doping density increases, it can elevate the rate of recombination and hinder carrier mobility, which negatively impacts Jsc.

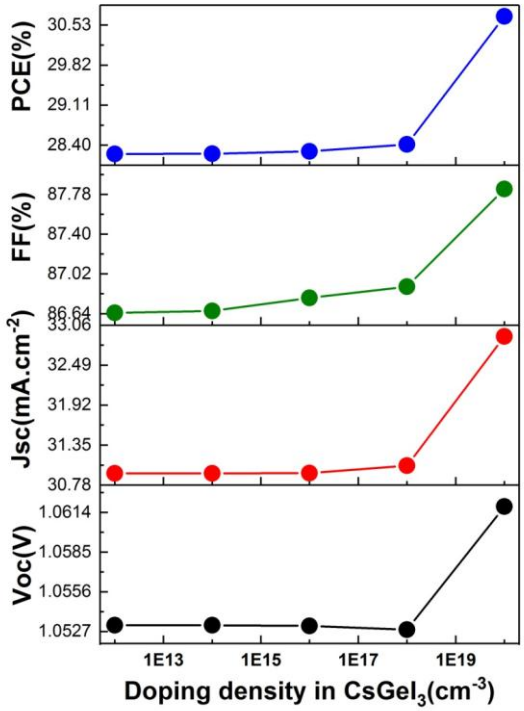

Figure 5: Solar cell characteristics as a function of $CsGeI_3$ doping density.

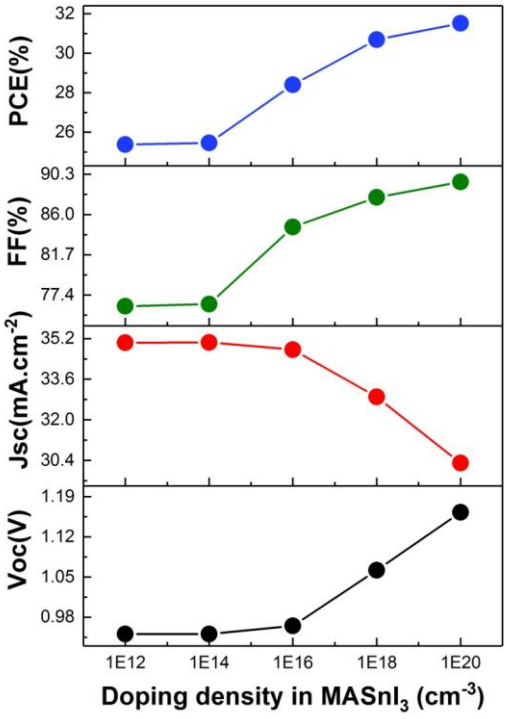

Figure 6: The solar cell characteristics as a function of $MASnI_3$ doping density.

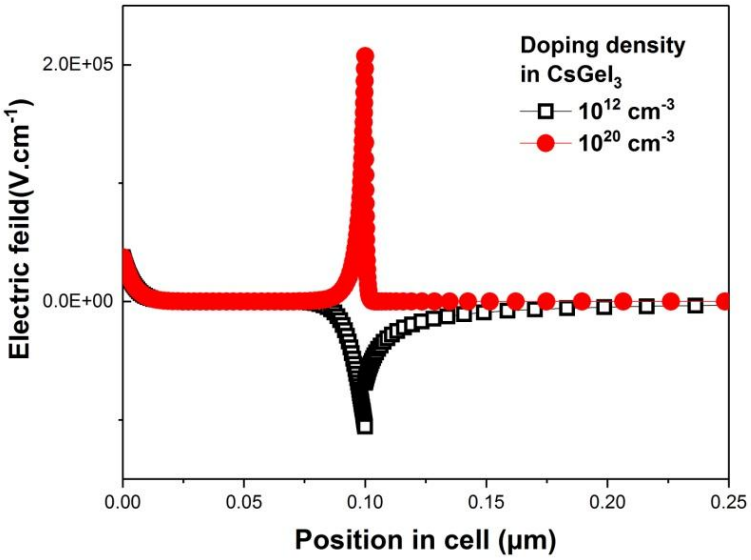

Figure 7: The electric field as a function of cell thickness for 10^{12} and 10^{20} cm^{-3} $CsGeI_3$ doping density.

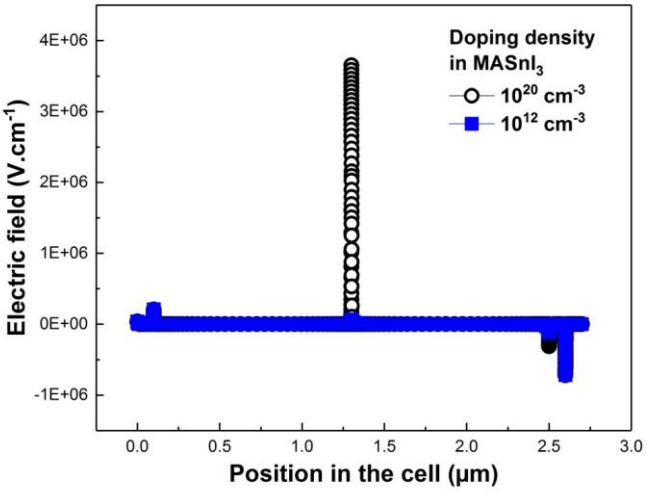

Figure 8: The electric field as a function of cell thickness for $10^{12}$and 10^{20}cm^{-3}$MASnI_3$ doping density.

However, the stronger built-in electric field and reduced recombination at interfaces (Figure 8), leading to improve Voc, FF, and PCE. Therefore, while Jsc may decline, the overall efficiency metrics can still improve due to better charge separation and collection. We chose 10^{20} cm^{-3} optimal doping density for $MASnI_3$ layer, in this value Voc=1.162697 V, Jsc=30.29736941 mA cm^{-2}, FF=89.4730%, and PCE=31.5183%. This value was used for the remaining simulation.

Optimization of defect density in$CsGeI_3$ and $MASnI_3$ layers

While it is unlikely to fabricate a perovskite solar cell completely free of defects, computational approaches such as density functional theory (DFT) have demonstrated the importance of defect engineering in solar cell material [29-30]. Therefore, it must be important to know in which way the defects affect the cell performance, to do that we varied the density of defects on each active layer from 10^{12} to 10^{20} cm^{-3}. Figure 9 demonstrates the influence of defect density at the$CsGeI_3$ layer on the solar cell characteristics. It was found that the defect density has almost no noticeable effect on cell performance.

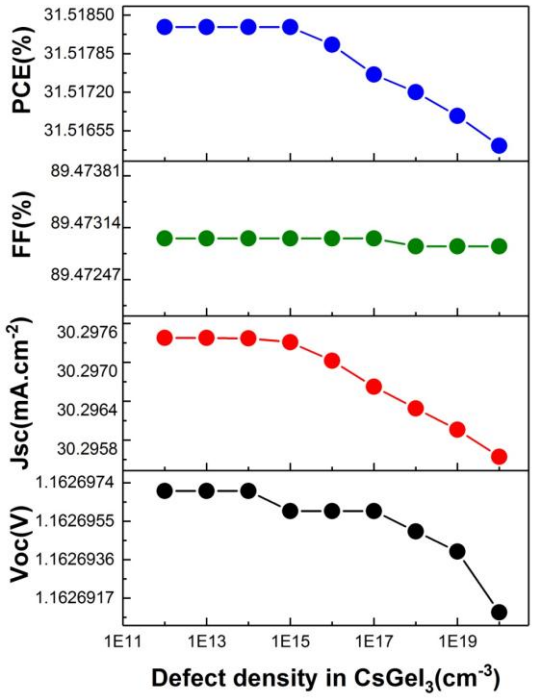

Figure 9: Variation in solar cell characteristics with changing defect density in the $CsGeI_3$ layer**.**

This layer has a lower density of recombination states, allowing it to maintain its performance even with increased defects. This was confirmed by plotting the Recombination rate at each cell position for defect densities 10^{12} cm^{-3}-10^{20} cm^{-3} in the $CsGeI_3$ layer; Figure 10 shows the resulting curves.

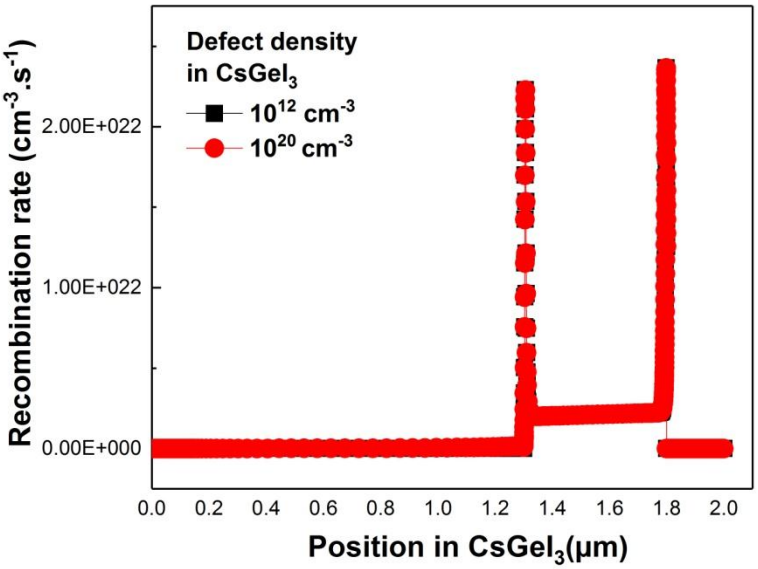

Figure 10: The rate of recombination as a function of position in the cell for the density of defects of 10^{12} and 10^{20} cm^{-3} in the $CsGeI_3$ layer.

Figure 11 describes the impact of defect density in the $MASnI_3$ on photovoltaic parameters. It was found that the increase in defect density declines the cell performance, at the lowest defect of $10^{12}cm^{-3}$, we record optimal values for the cell parameters: Voc=1.166439 V, Jsc=30.71706170 mA cm^{-2}, FF=89.5191%, and PCE=32.0743%. Afterwards, as the defect density increases, this performance decreases until it reaches its lowest value: Voc=0.895978 V, Jsc=0.65946628 mA cm^{-2}, FF=81.2593%, and PCE=0.4801% at the highest value of defect density 10^{20} cm^{-3}.

The $MASnI_3$ layer is often critical in final charge extraction. Increased defects in this layer can create trap states that hinder charge movement, leading to higher recombination rates and lower overall performance metrics [31], this behavior is illustrated in Figure 12 which shows the recombination rate at each cell position for defect densities 10^{12} cm^{-3} and 10^{20} cm^{-3} in $MASnI_3$ layer. However, we can report the effect of these defects does not become significant until after 10^{14} cm^{-3}.

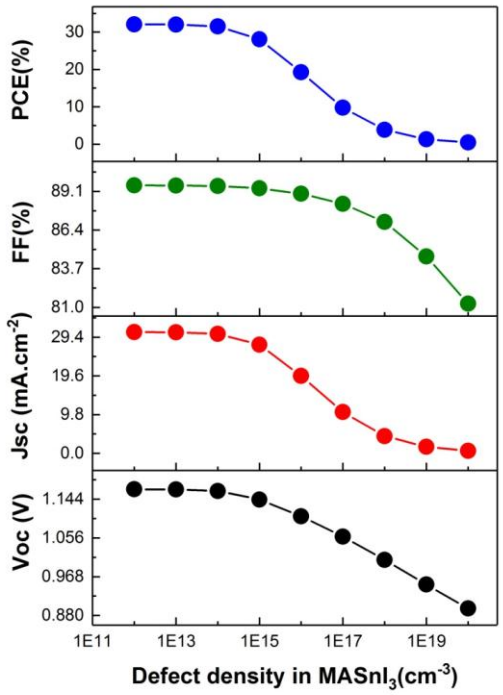

Figure 11: Variation in solar cell characteristics with changing defect density in the $MASnI_3$ layer.

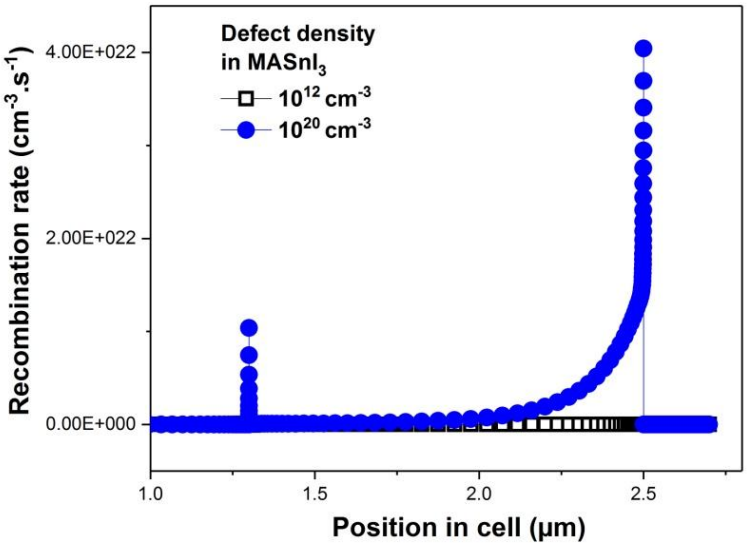

Figure 12: The recombination rate as a function of position in the cell for densities of defects of 10^{12} and 10^{20} cm^{-3} in the $MASnI_3$ layer.

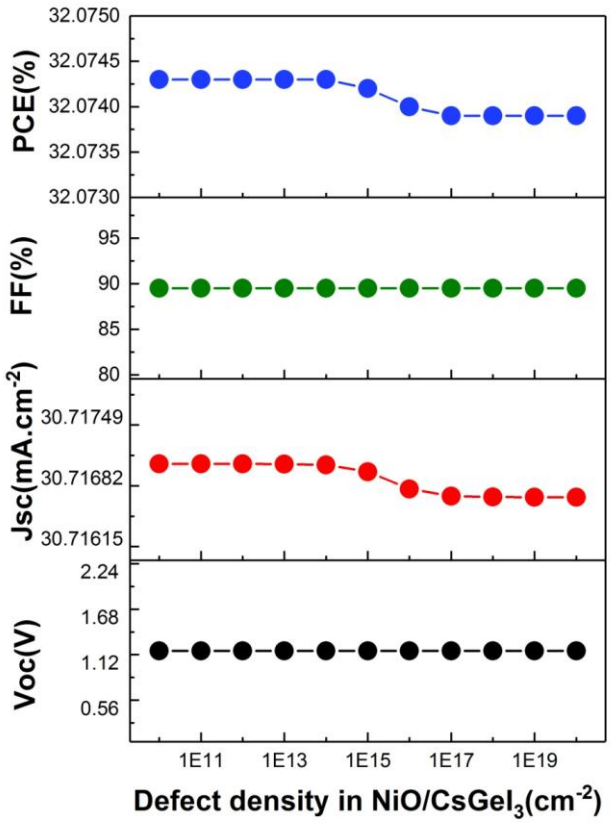

Figure 13: Variations of solar cell characteristics with changing defect density at the $NiO/CsGeI_3$ interface.

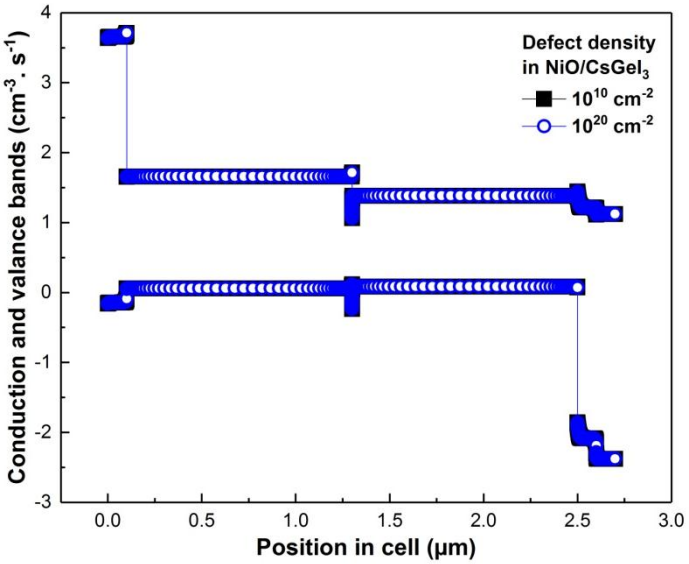

Figure 14: The conduction and valence band profiles across the cell for different defect densities at the $NiO/CsGeI_3$ interface.

Optimization of $NiO/CsGeI_3$; $CsGeI_3/MASnI_3$; $MASnI_3/ZnO$ interfaces defect density

The manufacturing process of PSCs can also introduce interface defects, such as grain boundaries and dangling bonds, at the interfaces [11,32]. Therefore, addressing interface defects is crucial for optimizing the efficiency of the cell. In this part, we studied the density of defects in ($NiO/CsGeI_3$; $CsGeI_3/MASnI_3$; $MASnI_3/ZnO$) interfaces, ranging from 10^{10} to 10^{20} cm^{-2}.

For the $NiO/CsGeI_3$ interface

Figure 13 indicates that there is no noticeable effect on cell performance.

This is because the defect density at the $NiO/CsGeI_3$ interface does not affect the conduction and valence band energy levels of the cell (Figure 14), that makes the charge carriers still move efficiently through the materials, and as a result, the performance remains stable.

For the $CsGeI_3/MASnI_3$interface

According to Figure 15, there is a small decrease in the PV parameters from 10^{10} to 10^{14} cm^{-2}, and then stabilize from $10^{14}$to 10^{20} cm^{-2}.

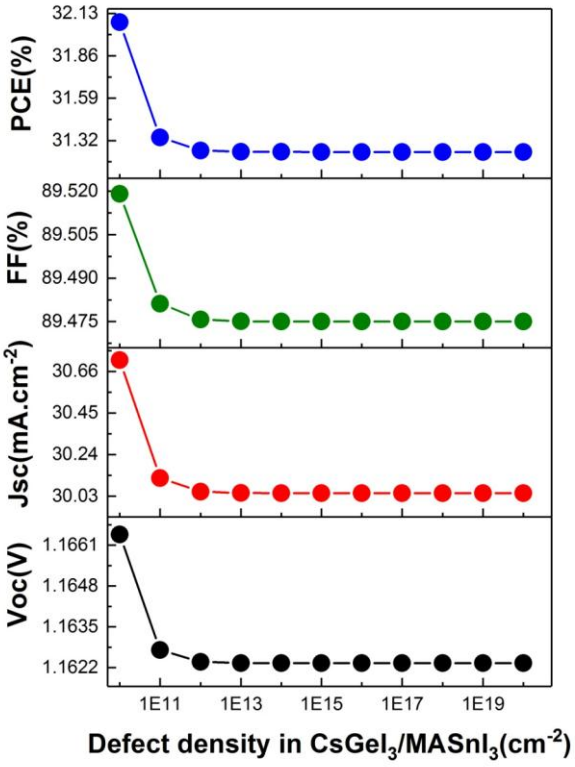

Figure 15: Variations of solar cell characteristics with changing defect density at the $CsGeI_3/MASnI_3$ interface.

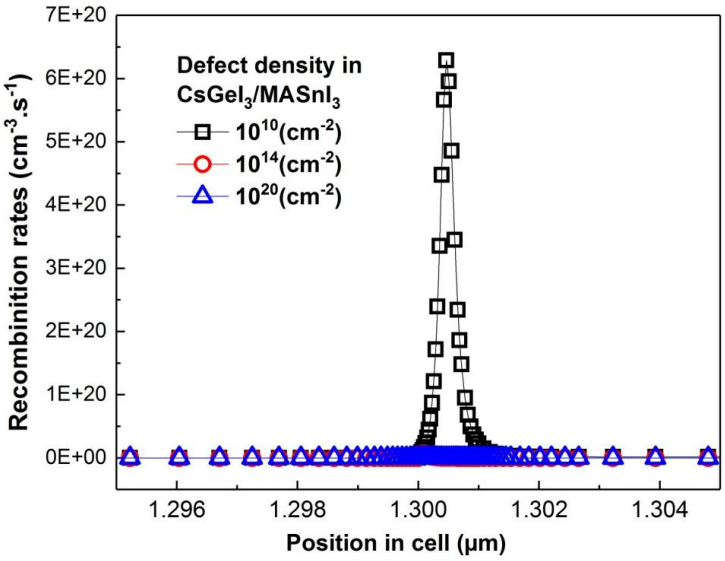

Figure 16: The change in recombination rate across the thickness of the cell at defect densities of 10^{10}, 10^{14} and 10^{20} cm^{-2} at the $CsGeI_3/MASnI_3$ interface.

As defect density increases beyond 10^{14} cm^{-2}, the interface may reach a state where the additional defects do not contribute significantly to further recombination losses. This could be to the fact that most of the available states for recombination are already occupied, leading to a stabilization of the PV parameters, this behavior was confirmed by the results observed in Figure 16, as there is no change in the recombination rate between the values for 10^{14} cm^{-2} and 10^{20} cm^{-2}.

For $MASnI_3/ZnO$ interface

As shown in Figure 17, when the defect density increases, the PV parameters decline rapidly from: Voc=1.166439 V, Jsc=30.71706170 mA cm^{-2}, FF=89.5191%, PCE=32.0743% to Voc=0.856759 V, Jsc=1.75326955 mA cm^{-2}, FF=79.8155%, and PCE=1.1989%.

Increasing the defect density at the $MASnI_3/ZnO$ interface alters the energy levels of the valence and conduction bands (as illustrated in Figure 18), these changes directly impact the cell performance.

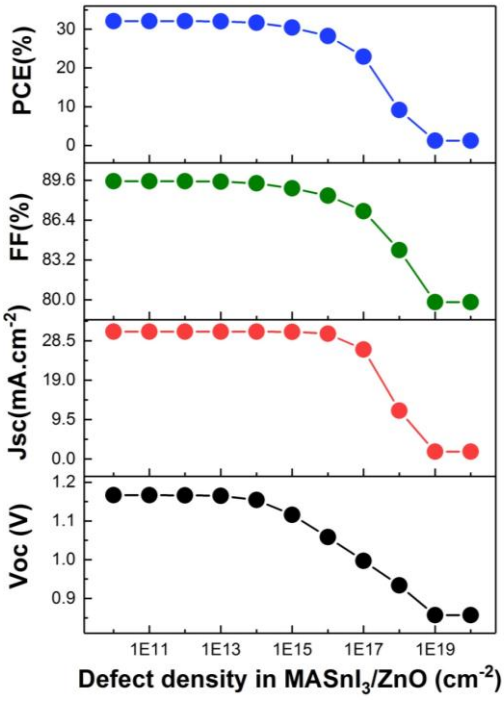

Figure 17: Variation of solar cell characteristics with changing defect density at the $MASnI_3/ZnO$ interface.

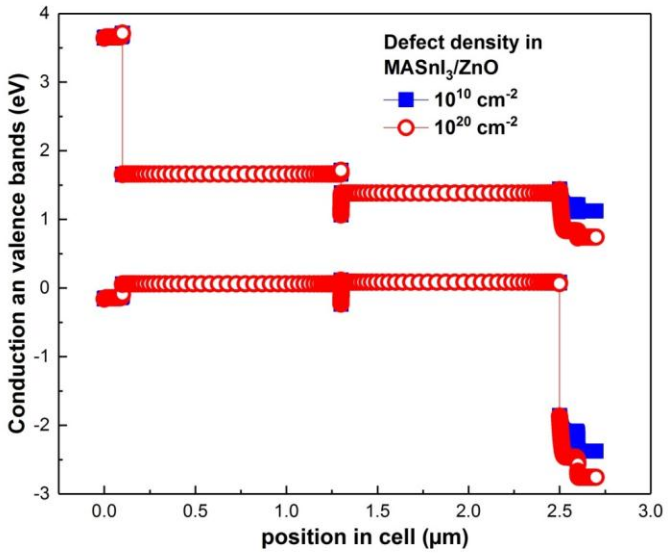

Figure 18: The conduction and valence bands across the cell for different defect densities at the $MASnI_3$/ZnO interface.

Stability and cost considerations

While this study focuses on optimizing photovoltaic performance, stability and cost remain critical for real-world adoption of perovskite solar cells. Based on material selection and literature, we analyze the stability and cost prospects of the proposed of our structure:

Cost analyses reveal that PSC modules can be produced at lower costs than other photovoltaic technologies with estimated manufacturing costs ranging from 28.7 $ to 42.3 $ per m^2 depending on the configuration [33], the leveled cost of electricity (LCOE) for PSCs is projected to be 3.5-4.9 US cent/KWh, assuming efficiencies above 12% and lifetimes exceeding 15 years [34]. Amore conservative estimate suggests LCOE value between 4.93-7.90 cents/KWh for modules with 16% efficiency in a 30-year utility-scale plant [35]. Tin and germanium perovskites exhibits reduced ion migration compared to lead-based analogs, a key degradation pathway in PSCs [3,13]. For instance, $CsGeI_3$ demonstrates improved phase stability under ambient conditions due to its stronger ionic bonding [15,36-37] while $MASnI_3$'s oxidation sensitivity can be mitigated through encapsulation [4]. The optimized defect density in the $MASnI_3$ layer minimizes the recombination processes, a key driver of instability, where improved annealing techniques, such as optimized temperature control, may contribute to reducing structural defects by enhancing crystallinity and grain alignment [38-39]. NiO and ZnO are inorganic charge transport layers known for their thermal and chemical stability, NiO's robustness against UV light and moisture [16], ZnO's low temperature deposition, reduces interfacial degradation. The p-i-n structure with NiO/ZnO layers outperforms n-i-p designs due to lower material costs and faster processing [35]. Further experimental work is pending to validate these predictions.

Conclusion

Through this research, a new structure of perovskite solar cell is proposed as a solution to the toxicity problem of lead-based perovskites while maintaining high yield, this structure has a double layer of perovskite composed of $MASnI_3$ and $CsGeI_3$ as active layers, with ZnO as ETL, NiO as HTL, and FTO as front contact. Using the SCAPS-1D simulator, the effect of several factors on the device performance was studied. The thickness of the active layers (optimized to 1200 nm).The doping density (10^{20} cm^{-3} for both layers) significantly

improved efficiency. Defect density analysis revealed that the $CsGeI_3$layerexhibited negligible performance degradation even at high defect densities (10^{20} cm^{-3}), while the $MASnI_3$ required a low defect density (10^{12} cm^{-3}) for optimal performance. Interface defect studies showed minimal impact at $NiO/CsGeI_3$ interface; however, severe efficiency losses at the $MASnI_3/ZnO$ interface for defects exceeding 10^{12} cm^{-2}. These optimizations achieved outstanding results: Voc=1.166439 V; Jsc=30.71706170 $mAcm^{-2}$; FF=89.5191%; and PCE=32.0743%, with the possibility for long-term stability. This research shows the potential of lead-free $CsGeI_3/MASnI_3$-based PSCs as a high-efficiency, cost-effective, and environmentally sustainable alternative to lead-based technologies, by addressing toxicity, cost, stability, this work positions lead-free perovskite as a cornerstone of next–generation photovoltaics. Future efforts should focus on experimental validation to confirm practical applicability, such as fabricating the proposed $FTO/ZnO/MASnI_3/CsGeI_3/NiO$ structure, focusing on defect-minimized interfaces and scalable deposition techniques, conduct accelerated aging tests under operational stressors (thermal cycling, humidity, and light soaking) to asses PCE retention and degradation pathways, explore advanced encapsulation approaches to mitigate to suppress Sn^{2+} oxidation.

Acknowledgements

The authors gratefully acknowledge the use of the SCAPS simulation software, which proved instrumental in facilitating this research. The SCAPS tool was generously provided by Prof. M. Burgeleman and his research group at the Department of Electronics and Information Systems (ELIS), University of Gent, Belgium. This work forms part of PRFU research project (Contract No: B00L02UUN310220001), supported by the Oran University of Science and technology-Mohamed Boudiaf (USTO-MB), Algeria.

Orcid

Abdullah Belbia: 0009-0001-2377-4768

Keltoum Dris: 0009-0009-4601-7565

Mostefa Benhaliliba: 0000-0001-6507-3663

Abbas Ayeshamariam: 0000-0003-3683-3488

Reference

[1]. J. Fan, B. Jia, M. Gu, Perovskite-based low-cost and high-efficiency hybrid halide solar cells, *Photonics Research*, **2014**, *2*, 111-120. [Google Scholar], [Publisher]

[2]. E.J. Chukwuemeka, N.A. Osita, A.O. Odira, U.C. Uchechukwu, J.D. Mimi, I.L. Ikhioya, Performance and stability evaluation of low-cost inorganic methyl ammonium lead iodide ($CH_3NH_3PbI_3$) perovskite solar cells enhanced with natural dyes from cashew and mango leaves, *Adv. J. Chem. Sect. A*, **2024**, *7*, 27-40. [Crossref], [Google Scholar], [Publisher]

[3]. E. Aktas, N. Rajamanickam, J. Pascual, S. Hu, M.H. Aldamasy, D. Di Girolamo, W. Li, G. Nasti, E. Martínez-Ferrero, A. Wakamiya, Challenges and strategies toward long-term stability of lead-free tin-based perovskite solar cells, *Communications Materials*, **2022**, *3*, 104. [Crossref], [Google Scholar], [Publisher]

[4]. T. Seyisi, B. Fouda-Mbanga, J. Mnyango, Y. Nthwane, B. Nyoni, S. Mhlanga, S. Hlangothi, Z. Tywabi-Ngeva, Major challenges for commercialization of perovskite solar cells: A critical review, *Energy Reports*, **2025**, *13*, 1400-1415. [Crossref], [Google Scholar], [Publisher]

[5]. Q. Ul Ain, J. Xia, H. Kanda, I.R. Alwani, X.X. Gao, H.U. Rehman, G. Shao, V. Jankauskas, K. Rakstys, A. Ahmed Khan, Transparent liquid crystal hole-transporting material for stable perovskite solar cells, *Solar Rrl*, **2023**, *7*, 2200920. [Crossref], [Google Scholar], [Publisher]

[6]. D. Di Girolamo, F. Matteocci, F.U. Kosasih, G. Chistiakova, W. Zuo, G. Divitini, L. Korte, C. Ducati, A. Di Carlo, D. Dini, Stability and dark hysteresis correlate in NiO-based perovskite solar cells, *Advanced Energy Materials*, **2019**, *9*,

1901642. [Crossref], [Google Scholar], [Publisher]
[7]. S. Bai, P. Da, C. Li, Z. Wang, Z. Yuan, F. Fu, M. Kawecki, X. Liu, N. Sakai, J.T.W. Wang, Planar perovskite solar cells with long-term stability using ionic liquid additives, *Nature*, **2019**, *571*, 245-250. [Crossref], [Google Scholar], [Publisher]
[8]. S. Chen, X. Xiao, H. Gu, J. Huang, Iodine reduction for reproducible and high-performance perovskite solar cells and modules, *Science Advances*, **2021**, *7*, eabe8130. [Crossref], [Google Scholar], [Publisher]
[9]. S. Mazumdar, Y. Zhao, X. Zhang, Stability of perovskite solar cells: Degradation mechanisms and remedies, *Frontiers in Electronics*, **2021**, *2*, 712785. [Crossref], [Google Scholar], [Publisher]
[10]. M. Sajjadnejad, S. Karkon, S.M.S. Haghshenas, Corrosion characteristics of Zn-TiO2 nanocomposite coatings fabricated by electro-codeposition process, *Advanced Journal of Chemistry, Section A*, **2024**, *7*, 209-226. [Crossref], [Google Scholar], [Publisher]
[11]. K. Dris, M. Benhaliliba, Study and Optimization of a New Perovskite Solar Cell Structure Based on the Two Absorber Materials Cs2TiBr6 and MASnBr3 Using SCAPS 1D, *Periodica Polytechnica Chemical Engineering*, **2024**, *68*, 348-363. [Crossref], [Google Scholar], [Publisher]
[12]. W. Ke, M.G. Kanatzidis, Prospects for low-toxicity lead-free perovskite solar cells, *Nature communications*, **2019**, *10*, 965. [Crossref], [Google Scholar], [Publisher]
[13]. H. Alipour, A. Ghadimi, Optimization of lead-free perovskite solar cells in normal-structure with WO3 and water-free PEDOT: PSS composite for hole transport layer by SCAPS-1D simulation, *Optical Materials*, **2021**, *120*, 111432. [Crossref], [Google Scholar], [Publisher]
[14]. S.T. Thornton, G. Abdelmageed, R.F. Kahwagi, G.I. Koleilat, Progress towards l ead-free, efficient, and stable perovskite solar cells, *Journal of Chemical Technology & Biotechnology*, **2022**, *97*, 810-829. [Crossref], [Google Scholar], [Publisher]
[15]. X. Zhang, T. Li, C. Hu, Z. Fu, J. Lin, Z. Cheng, J. Wu, Y. Qi, Y. Ruan, L. Huang, Investigation of efficient all-inorganic HTL-free CsGeI3 perovskite solar cells by device simulation, *Materials Today Communications*, **2023**, *34*, 105347. [Crossref], [Google Scholar], [Publisher]
[16]. F. Jafarzadeh, L.A. Castriotta, E. Calabrò, P. Spinelli, A. Generosi, B. Paci, D. Becerril Rodriguez, M. Luce, A. Cricenti, F. Di Giacomo, Stable and sustainable perovskite solar modules by optimizing blade coating nickel oxide deposition over 15× 15 cm2 area, *Communications Materials*, **2024**, *5*, 186. [Crossref], [Google Scholar], [Publisher]
[17]. M. Burgelman, P. Nollet, S. Degrave, Modelling polycrystalline semiconductor solar cells, *Thin solid films*, **2000**, *361*, 527-532. [Crossref], [Google Scholar], [Publisher]
[18]. K. Dris, M. Benhaliliba, Novel inorganic–organic heterojunction solar cell-based perovskite using two absorbent materials, *Nano*, **2023**, *18*, 2350091. [Crossref], [Google Scholar], [Publisher]
[19]. S.S. Madani, Investigation of charge transport metal oxides for efficient and stable perovskite solar cells, *Queensland University of Technology*, **2022**. [Crossref], [Google Scholar], [Publisher]
[20]. S. Mattaparthi, D.K. Sinha, A. Bhura, R. Khosla, Design of an eco-friendly perovskite Au/NiO/FASnI3/ZnO0. 25S0. 75/FTO, device structure for solar cell applications using SCAPS-1D, *Results in Optics*, **2023**, *12*, 100444. [Crossref], [Google Scholar], [Publisher]
[21]. K. Dris, M. Benhaliliba, Study and Optimization of a New Perovskite Solar Cell Structure Based on the Two Absorber Materials Cs2TiBr6 and MASnBr3 Using SCAPS 1D, *Periodica Polytechnica Chemical Engineering*,

2024, *68*, 348-363. [Crossref], [Google Scholar], [Publisher]
[22]. I. Sumbel, E. Raza, Z. Ahmad, M. Zubair, M.Q. Mehmood, H. Mehmood, Y. Massoud, M.M. Rehman, Numerical simulation to optimize the efficiency of HTM-free perovskite solar cells by ETM engineering, **2023**. [Crossref], [Google Scholar], [Publisher]
[23]. V. Gusak, B. Kasemo, C. Hagglund, Thickness dependence of plasmonic charge carrier generation in ultrathin a-Si: H layers for solar cells, *ACS nano*, **2011**, *5*, 6218-6225. [Crossref], [Google Scholar], [Publisher]
[24]. A. Mortadi, E. El Hafidi, M. Monkade, R. El Moznine, Investigating the influence of absorber layer thickness on the performance of perovskite solar cells: a combined simulation and impedance spectroscopy study, *Materials Science for Energy Technologies*, **2024**, *7*, 158-165. [Crossref], [Google Scholar], [Publisher]
[25]. M.A. Haque, D. Rosas Villalva, L.H. Hernandez, R. Tounesi, S. Jang, D. Baran, Role of dopants in organic and halide perovskite energy conversion devices, *Chemistry of Materials*, **2021**, *33*, 8147-8172. [Crossref], [Google Scholar], [Publisher]
[26]. J. Zhang, X. Gan, H. Sun, H. Yuan, L. Yu, Z. Hu, Y. Zhu, Pb-site doping of lead halide perovskites for efficient solar cells, *Solar RRL*, **2020**, *4*, 1900227. [Crossref], [Google Scholar], [Publisher]
[27]. V.C. Onuabuchi, A. Ullah, N.J. Opene, Y. Tai, C.I. Elekalachi, N.L. Okoli, Effect of deposition potential on the structural and optical properties of electrodeposited antimony doped zinc telluride (Sb: ZnTe) thin films for optoelectronic applications, *Journal of Medicinal and Nanomaterials Chemistry*, **2024**, *6*, 46. [Crossref], [Google Scholar], [Publisher]
[28]. E.N. Josephine, O.S. Ikponmwosa, T. Alomayri, I.L. Ikhioya, Enhanced physical properties of SnS/SnO semiconductor material, *Journal of Medicinal and Nanomaterials Chemistry*, **2023**, *5*, 199. [Crossref], [Google Scholar], [Publisher]
[29]. B. Semire, K.G. Obiyenwa, W.O. Anthony, K. Abubakar, M.A. Godwin, S.O. Fagbenro, S. Olusegun, O.W.S. Afolabi, Manipulation of 2-[2-(10H-phenothiazin-3-yl) thiophen-3-yl]-10H-phenothiazine based DA-π-a dyes for effective tuning of optoelectronic properties and intramolecular charge transfer in dye sensitized solar cells: A DFT/TD-DFT approach, *J. Chem. A*, **2024**, *7*, 41-58. [Crossref], [Google Scholar], [Publisher]
[30]. Z. Guo, M. Yuan, G. Chen, F. Liu, R. Lu, W.J. Yin, Understanding defects in perovskite solar cells through computation: current knowledge and future challenge, *Advanced Science*, **2024**, *11*, 2305799. [Crossref], [Google Scholar], [Publisher]
[31]. K. Dris, M. Benhaliliba, A. Ayeshamariam, A. Roy, K. Kaviyarasu, Improving the perovskite solar cell by insertion of methyl ammonium tin oxide and cesium tin chloride as absorber layers: Scaps 1d study based on experimental studies, *Journal of Optics*, **2024**, 1-23. [Crossref], [Google Scholar], [Publisher]
[32]. M.M. Haque, S. Mahjabin, S. Khan, M.I. Hossain, G. Muhammad, M. Shahiduzzaman, K. Sopian, M. Akhtaruzzaman, Study on the interface defects of eco-friendly perovskite solar cells, *Solar Energy*, **2022**, *247*, 96-108. [Crossref], [Google Scholar], [Publisher]
[33]. Z. Song, A.B. Phillips, I. Celik, G.K. Liyanage, D. Zhao, D. Apul, Y. Yan, M.J. Heben, Manufacturing cost analysis of perovskite solar modules in single-junction and all-perovskite tandem configurations, *2018 IEEE 7th World Conference on Photovoltaic Energy Conversion (WCPEC)(A Joint Conference of 45th IEEE PVSC, 28th PVSEC & 34th EU PVSEC)*, *IEEE*, **2018**, 1134-1138. [Crossref], [Google Scholar], [Publisher]
[34]. M. Cai, Y. Wu, H. Chen, X. Yang, Y. Qiang, L. Han, Cost-performance analysis of perovskite solar modules, *Advanced Science*, **2017**, *4*,

1600269. [Crossref], [Google Scholar], [Publisher]
[35]. Z. Song, C.L. McElvany, A.B. Phillips, I. Celik, P.W. Krantz, S.C. Watthage, G.K. Liyanage, D. Apul, M.J. Heben, A technoeconomic analysis of perovskite solar module manufacturing with low-cost materials and techniques, *Energy & Environmental Science*, **2017**, *10*, 1297-1305. [Crossref], [Google Scholar], [Publisher]
[36]. T. Krishnamoorthy, H. Ding, C. Yan, W.L. Leong, T. Baikie, Z. Zhang, M. Sherburne, S. Li, M. Asta, N. Mathews, Lead-free germanium iodide perovskite materials for photovoltaic applications, *Journal of Materials Chemistry A*, **2015**, *3*, 23829-23832. [Crossref], [Google Scholar], [Publisher]
[37]. A. W. Azhari, F. Shi, X. Then, D. Suriyani, C. Halin, and S. Sepeai, Tin and germanium substitution in lead free perovskite solar cell: current status and future trends, *IOP Conference Series: Materials Science and Engineering,* **2020**, 957, 01205, 1-6. [Google Scholar], [Publisher]
[38]. I. Ahmad, J. Razzaq, A. Ammara, F. Kaleem, M. Qamar, S. Ilahi, I.L. Ikhioya, Impact of annealing temperature on hydrothermally synthesized copper antimony oxide (Cu2Sb2O) from amorphous phase to monoclinic structure, *Advanced Journal of Chemistry, Section A*, **2024**, *7*, 110-121. [Crossref], [Google Scholar], [Publisher]
[39]. I.L. Ikhioya, N.I. Akpu, E.U. Onoh, S.O. Aisida, I. Ahmad, M. Maaza, F.I. Ezema, Impact of precursor temperature on physical properties of molybdenum doped nickel telluride metal chalcogenide material, *Journal of Medicinal and Nanomaterials Chemistry*, **2023**. [Crossref], [Google Scholar], [Publisher]